

Spatiotemporal Variability Analysis of Water Hyacinth (*Eichhornia crassipes*) and Its Impact on the Lake Tana Ecosystem Using Remote Sensing Technology

リモートセンシング技術を使用したエチオピアのタナ湖におけるホテイアオイ (*Eichhornia crassipes*) の時空間的変動解析とその影響

Student ID:22D5803

Name: Getachew Bayable Tiruneh

Supervisor: Victor S. Kuwahara

SYNOPSIS

This study examined the spatiotemporal dynamics of water hyacinth (WH) and its impact on hydrology and water quality in Lake Tana, Ethiopia. Three non-parametric machine learning algorithms were evaluated for WH detection. All classifiers achieved >95% accuracy with Sentinel-2 and >90% with Landsat-8. Although the performance differences between the methods were small, Random Forest demonstrated the highest accuracy and was used to estimate the spatiotemporal variability of WH distribution. High WH populations were concentrated in Lake Tana's northeastern sector, with spatial coverage increasing significantly from 2015 to 2023. Water loss due to WH evapotranspiration also increased significantly during this period. Lake surface water temperature (LSWT) decreased significantly across all seasons except the dry season. Turbidity declined significantly in all seasons except the pre-rainy season. Chlorophyll-*a* (Chl-*a*) decreased in pre-rainy and rainy seasons but showed a non-significant increasing trend during dry and post-rainy seasons. WH biomass had a non-significant positive correlation with LSWT ($r = 0.18$), while a significant negative correlation with turbidity ($r = -0.33$) and Chl-*a* ($r = -0.35$). This study identified RF as the most accurate method for WH detection and comprehensively quantified its spatiotemporal distribution and impacts on the ecosystem using remote sensing technology for the first time.

Keywords: Chlorophyll-*a*, lake surface water temperature, satellite imagery, turbidity, water hyacinth

1. Introduction

Water is the most important resource on Earth, providing essential socio-economic and ecological benefits¹. However, freshwater resources are steadily declining due to pollution, agricultural expansion, urbanization, climate change, and poor watershed management. These factors contribute to lake eutrophication and the spread of invasive aquatic weeds such as water hyacinth (WH)^{2,3}.

WH is a major concern for environmentalists and water resource managers due to its negative effects on aquatic life, ecosystems, and human livelihoods¹. It disrupts habitats, food chains, nutrient cycles, and aquatic communities, impacting the entire food web⁴. The International Union for Conservation of Nature (IUCN) ranks WH among the top 100 most harmful invasive species⁵, and it is considered one of the top 10 worst weeds globally⁶. In tropical highland lakes like Lake Tana in Ethiopia, WH affects biodiversity, fisheries, navigation, tourism, and water quality⁷. It also leads to water loss due to higher evapotranspiration rates in WH-infested areas⁸. However, in its native ecosystems, WH enhances habitat complexity, provides shelter and feeding grounds, and aids in water purification through pollutant absorption^{9,10}. A comprehensive understanding of WH's distribution and ecological impact is essential for developing balanced strategies that mitigate its harmful effects while acknowledging its potential benefits in native ecosystems.

Physical and biological water quality parameters, such as lake surface water temperature (LSWT), turbidity, and Chlorophyll-*a* (Chl-*a*), are crucial for assessing lake health and ecosystem dynamics. LSWT regulates various physical, chemical, and biological processes in aquatic ecosystems¹¹, turbidity indicates sedimentation¹², and Chl-*a* reflects the lake's nutritional status¹³. Since these parameters can be influenced by WH infestation, monitoring their relationship with WH biomass is essential for sustainable lake ecosystem management.

Traditional field surveys are costly and time-consuming. Satellite data provides a more efficient solution for monitoring WH distribution and water quality without geographical constraints¹. Satellite imagery, combined with *in-situ* measurements, allows for frequent and large-scale monitoring of LSWT, turbidity, and Chl-*a*¹⁴. MODIS is particularly useful for LSWT estimation due to its high accuracy and extensive temporal coverage¹⁵, while Sentinel-2 offers improved accuracy

for turbidity and Chl-*a* retrieval¹⁶. Common machine learning algorithms such as Classification and Regression Tree (CART), Random Forest (RF), and Support Vector Machine (SVM) are widely used for satellite image classification because of their efficiency and accuracy when compared with parametric algorithms like maximum likelihood classifiers^{17,18}. Deep learning techniques, such as convolutional neural networks (CNNs), also show promising results for image classification tasks. However, they are computationally intensive and require extensive ground truth training data. Comparing common machine learning algorithms can help identify the most effective method for detecting WH in Lake Tana.

Previous studies on WH spatiotemporal distribution in Lake Tana have mainly relied on parametric algorithms using spectral bands. Abebe et al.¹⁹, manually digitized WH from Sentinel-2 imagery but had difficulty in distinguishing it from other aquatic vegetation. Most studies in the lake used maximum likelihood classifiers, and lower resolution Landsat (5 and 8) imagery, and were conducted before 2019. Given potential changes in WH distribution since 2019, updated information is crucial for developing effective management strategies. Water loss due to WH evapotranspiration has not been thoroughly explored; existing studies in Lake Tana^{8,19} used WH plant coefficients from other regions, highlighting the need for further research with region-specific coefficients. Research on the spatiotemporal variability of physical and biological water quality parameters, such as LSWT, turbidity, and Chl-*a*, is spatially limited and temporally fragmented³. Further, the relationship between WH biomass and water quality parameters has not been thoroughly investigated. Therefore, the overall objective of this doctoral research was to analyze the spatiotemporal distribution of WH and its impact on hydrology and water quality using remote sensing technology. Specifically, the study aimed to *i) Study 1*: compare the performance of three non-parametric machine-learning algorithms (RF, SVM, and CART) for WH detection, *ii) Study 2*: analyze the spatiotemporal dynamics of WH and associated water loss due to evapotranspiration from 2015 to 2023, and *iii) Study 3*: examine the spatiotemporal distribution of physical and biological water quality parameters and their interrelationship with WH biomass.

2. Materials and Methods

Study 1: Detection of water hyacinth (*Eichhornia crassipes*) in Lake Tana, Ethiopia, using machine learning algorithms

Data and processing: Cloud-masked monthly median composite images from Level-2A processed Landsat-8 and Sentinel-2, acquired in October 2021, January 2022, March 2022, and June 2022, were used to represent the post-rainy, dry, pre-rainy, and rainy seasons, respectively. Spectral bands and various indices were also used as input for the classifiers. First, nine spectral indices were generated: Normalized Difference Vegetation Index (NDVI), Enhanced Vegetation Index (EVI), Chlorophyll Index Green (CIG), Normalized Difference Water Index (NDWI), Simple Ratio Index (SRI), Modified Normalized Difference Water Index (MNDWI), Green Normalized Difference Vegetation Index (GNDVI), Optimized Soil Adjusted Vegetation Index (OSAVI), and Difference Vegetation Index (DVI). Pairwise correlation analysis was performed to reduce redundancy and identify less correlated indices. Five highly correlated indices (GNDVI, OSAVI, DVI, EVI, and CIG) were removed. The remaining four less correlated indices (NDVI, SRI, NDWI, and MNDWI) were used as classifier inputs along spectral bands.

Sample point generation methods and accuracy assessment: Images were classified into four land use/cover (LULC) classes: water, WH, other vegetation, and bare land. Field visits, GPS points, and visual interpretation of Landsat-8 and Sentinel-2 images, with the help of high-resolution Google Earth images, expert opinions, and reports from the Lake Tana Protection and Development Agency (LTPDA), were used to digitize and delineate these classes manually. A stratified random sampling method was used within these delineated polygons to generate 1200 labeled samples (300 for each class), with 70% for training and 30% for validation. Three non-parametric machine learning methods available in Google Earth Engine (GEE)—CART, RF, and SVM—were used to evaluate WH detection. Hyperparameter tuning was performed for CART (minimum observations per leaf, maximum nodes), RF (number of trees, bag fraction), and SVM (cost parameter, linear kernel). Individual validation sample points were used to evaluate the performance of the classifier. The performance of the three classifiers was evaluated using overall accuracy, *Kappa* coefficient, user accuracy (equivalent to precision), producer accuracy (corresponding to recall), and F1 score. Spectral reflectance curves of WH were also analyzed to identify the optimal bands for distinguishing WH from other LULC types.

Study 2: Spatiotemporal dynamics of water hyacinth (WH) and associated water loss due to its evapotranspiration in Lake Tana

Data and processing: Cloud-masked Sentinel-2 Level-1C imagery was used, along with the spectral bands and four indices that were selected in Study 1.

Sample point generation methods and WH mapping: Images were classified into water, WH, and other LULC classes. Manual digitization and delineation of these classes were performed on Sentinel-2 images using field visits, visual interpretation, Google Earth images, expert opinions, and LTPDA reports. Various experiments were conducted using a trial-and-error approach to identify the optimal number of training samples for achieving high classification accuracy. A total of 1,800 labeled samples—800 for water, 400 for WH, and 600 for other LULC classes—were generated using the stratified random sampling method, with 70% allocated for training and 30% for validation, resulting in high classification accuracy. The RF algorithm was used to map the spatial and temporal distribution of WH from 2015 to 2023 due to its superior accuracy (Study 1). WH spatial coverage was calculated using the grouped reducer and *reduceRegion()* function in GEE. Each RF-classified image was assessed using the evaluation metrics mentioned in Study 1. The annual expansion rate was calculated by comparing the maximum WH coverage between consecutive years.

Estimation of water loss due to WH: To estimate water loss due to WH evapotranspiration, data on open water evaporation

(Ev), WH evapotranspiration (ET_{wh}), and the spatial coverage of WH were required. MODIS potential evapotranspiration (PET) data from NASA's AppEEARS was used to estimate Ev. Since actual Ev is typically lower than PET, it was estimated at 80% of PET based on USGS research²⁰. MODIS-based Ev for Lake Tana showed a strong correlation ($r = 0.82$) with data from the National Meteorological Agency of Bahir Dar⁸, confirming its suitability. The plant coefficient (K_c) of water hyacinth ranges from 0.65 to 9.8 in the literature, with the FAO citing values of 1.1 (light to moderate wind) to 1.15 (strong wind) for tropical and subtropical regions²¹. A study in Lake Zeway, Ethiopia, reported a K_c value of 1.42 for WH²². This value was applied to Lake Tana due to its relevance to Ethiopian conditions. ET_{wh} was calculated as; $ET_{wh} = Ev \times K_c$ ²³. Water loss due to WH evapotranspiration was then estimated as; $Water\ loss = (ET_{wh} \times WH\ area) \times 0.001$ ²³, where water loss is in m³, area in m², and ET_{wh} in mm.

Study 3: Spatiotemporal variability of lake surface water temperature and water quality parameters and its interrelationship with water hyacinth biomass in Lake Tana, Ethiopia

Data and processing: Temperature, turbidity, and Chl-*a* were measured using a portable temperature logger, a LaMotte 2020t/i turbidimeter, and a KRK Kasahara CHL-30N Chl-*a* sensor, respectively, during the periods of December 6-10, 2022, and May 29-June 9, 2023, for validation. MODIS Terra LSWT (2001-2022) was used to estimate LSWT, while Sentinel-2 MSI (2016-2022) was used for turbidity, Chl-*a*, and WH biomass estimation.

WH biomass and remote sensing water quality indices: WH biomass was estimated from Sentinel-2 NDVI with a 0.6 threshold value. Turbidity and Chl-*a* were estimated from the Sentinel-2 Normalized Difference Turbidity Index (NDTI) and the Normalized Difference Chlorophyll Index (NDCI) from Sentinel-2 images, respectively.

Validation: MODIS LSWT was validated with *in-situ* water temperature measurements, showing a significant positive correlation ($r = 0.90$, $n = 38$). Sentinel-2 water quality indices, NDTI and NDCI, were validated with *in-situ* data, demonstrating strong positive correlations: NDTI with turbidity ($r = 0.92$, $n = 57$) and NDCI with Chl-*a* ($r = 0.84$, $n = 27$). Quadratic polynomial regression models, developed using *in-situ* measurements and Sentinel-2 data, were used to estimate turbidity and Chl-*a* values. However, limitations in *in-situ* data availability hindered robust long-term modeling of turbidity and Chl-*a* across all seasons. Thus, NDTI and NDCI were used for time series analysis of turbidity and Chl-*a*.

Trend detection and correlation analysis: Trend detection was performed using pixel-level linear regression, Innovative Trend Analysis (ITA), the Modified Mann-Kendall (MMK) trend test, and Sen's Slope Estimator. Pearson correlation coefficients and regression analysis were used to explore statistical relationships between WH biomass and water quality parameters.

3. Results and Discussion

Study 1: Detection of water hyacinth (*Eichhornia crassipes*) in Lake Tana, Ethiopia, using machine learning algorithms

WH exhibited the highest reflectance values in the red edge 2 (B6), red edge 3 (B7), near-infrared (B8), and red edge 4 (B8A) bands of Sentinel-2 imagery compared to other land use/land cover (LULC) types during the post-rainy, dry, and pre-rainy seasons. However, during the rainy season, WH reflectance in the B6, B7, B8, and B8A bands was lower than that of forest and grazing land

RF, CART, and SVM machine learning algorithms could detect and distinguish WH in Lake Tana using both Sentinel-2 and Landsat-8 images. However, SVM and CART misclassified some other vegetation types as WH, likely due to the similar spectral reflectance between dense vegetation and WH. Some water was also misclassified as other vegetation by the CART

and RF classifiers, with this issue being more prevalent in the CART classifier, possibly due to the high concentration of algae or phytoplankton in the lake water. Overall, the RF algorithm demonstrated higher accuracy in detecting WH than SVM and CART across all seasons and in both Landsat-8 and Sentinel-2 images.

All classification methods—CART, RF, and SVM—achieved >95% overall accuracy with Sentinel-2 images and > 90% with Landsat-8 images for WH mapping (Figure 1). The RF algorithm had the highest average overall accuracy at 98.31%, followed by SVM at 97.6% and CART at 97.5% in Sentinel-2 images. In Landsat-8 images, RF also achieved the highest average overall accuracy at 96.8%, followed by CART at 95% and SVM at 94.8%. Although the performance differences between the methods were small, RF achieved the highest precision, recall, F1 score, and overall accuracy (Figure 1) and was used to determine the spatial coverage of WH in *Study 2*. The average overall accuracy of the classifiers using Sentinel-2 images was 97.8%, while the average overall accuracy using Landsat 8 images was 95.5%. Although the difference in accuracy between the two types of satellite imagery was not significant, there was a meaningful difference in the estimation of WH area coverage. All methods achieved an F1 score >93% for WH detection with both Sentinel-2 and Landsat-8 images. However, F1 scores for WH detection were consistently lower with Landsat-8 images compared to Sentinel-2 images across all seasons and classifiers. This could be attributed to the presence of red edge bands and the higher spatial resolution of Sentinel-2 imagery (10-20 m), which allowed for better detection of WH compared to Landsat-8 imagery (30 m).

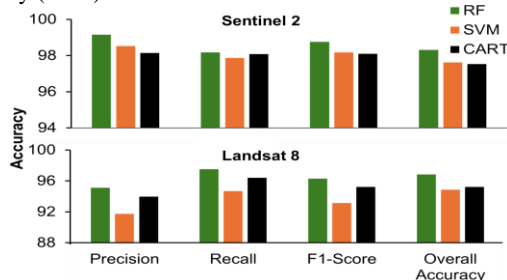


Figure 1. Average precision, recall, F1- score, and overall accuracy of the three classifiers for Sentinel-2 MSI and Landsat-8 OLI imagery.

During the post-rainy season, the WH class achieved the highest F1 score across all classifiers. However, the F1 score and κ coefficient (KC) were lowest during the dry season for Sentinel-2 images and during the dry and pre-rainy seasons for Landsat-8 images. The reduced F1 score and KC during the dry season were likely due to the presence of irrigated crops around Lake Tana, which have similar reflectance values to WH, making it difficult to distinguish between the two. Additionally, WH leaves change color and become dry during these seasons, altering their reflectance and further affecting classification accuracy. In contrast, when WH turns bright green (high reflectance) in the post-rainy season, detection accuracy increases significantly. These results underscore the post-rainy season as the optimum period for accurately detecting WH, leveraging its distinct spectral characteristics to improve classification performance.

Study 2: Spatiotemporal dynamics of water hyacinth (WH) and associated water loss due to its evapotranspiration in Lake Tana.

WH weeds are mainly found in the northeastern and eastern parts of Lake Tana, with the most severe infestation in the northeastern section of the lake. The high WH populations in these areas (Figure 2) could be associated with favorable environmental conditions, such as optimal levels of total nitrogen, total phosphorus, pH, salinity, temperature, and depth⁶. Besides, prevailing westerly winds, which blow eastward for much of the year can carry fragmented WH mats toward the northeastern part

of the lake³. This movement concentrates WH in this region and restricts its spread to other areas.

WH's annual maximum spatial coverage of the whole lake varied over time, ranging from 2.81 km² in November 2015 to 24.69 km² in November 2019 (Table 1). The spatial coverage of WH increased significantly at a rate of 0.06 km²/month from 2015 to 2023 ($P < 0.05$), peaking during the post-rainy season and reaching a minimum in the pre-rainy season. The peak spatial coverage in the post-rainy season could be attributed to nutrient runoff during the rainy season, driven by expanded cultivated land in the Tana Basin, which boosts WH growth as it takes time to respond to the enhanced nutrient availability. The annual maximum WH spatial coverage expansion rates increased from 2015 to 2019 (Table 1).

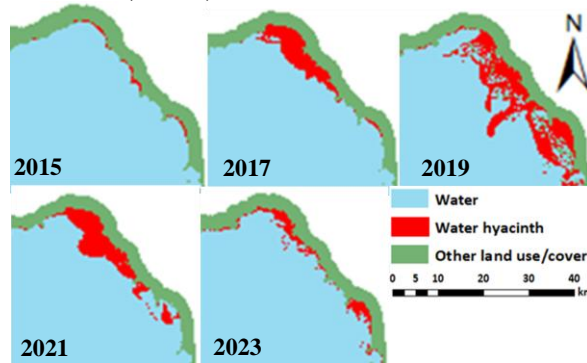


Figure 2. Spatiotemporal distribution of water hyacinth in the northeastern section of Lake Tana, showing maximum spatial coverage of WH.

However, the annual maximum WH spatial coverage expansion rate decreased by 4%, 1%, and 52% during 2020, 2021, and 2022 (Table 1), respectively, likely due to WH removal efforts, with approximately 80% of the weed in the lake removed in December 2020 (LTPDA, 2020²⁴). Overall, the WH annual maximum spatial coverage expansion rate increased by 439% from 2015 to 2023. Similarly, the annual maximum water surface area expansion rate increased slightly by 0.03% over the same period.

Table 1. Annual maximum (Max.) water hyacinth spatial coverage, lake surface area, and expansion rates (2015–2023) for the whole of Lake Tana.

Year	Annual Max. WH Area (km ²)	Expansion Rate (%)	Annual Max. Water Surface Area (km ²)	Expansion Rate (%)
2015	2.81	-	3042.79	-
2016	4.98	77	3047.04	0.14
2017	11.26	126	3045.59	-0.05
2018	20.86	85	3041.83	-0.12
2019	24.69	18	3035.97	-0.19
2020	23.58	-4	3061.54	0.84
2021	23.35	-1	3063.63	0.07
2022	11.10	-52	3056.47	-0.23
2023	15.13	36	3043.60	-0.42

Monthly water loss due to WH evapotranspiration ranged from 0.25 million m³ in June 2016 to 5.56 million m³ in October 2021, with a mean of 2.12 million m³. The rate of water loss due to WH evapotranspiration increased significantly at 0.014 million m³/month ($P < 0.05$). Water loss due to WH evapotranspiration was highest in the post-rainy season and lowest in the pre-rainy season. From October 2015 to December 2023, Lake Tana lost about 176 million m³ of water due to WH evapotranspiration, about 0.61% of its total lake volume (28.4 billion m³)¹⁹. This water loss also accounts for approximately 44.87% of Ethiopia's annual hydropower water consumption (0.4 billion m³/year)²⁵, 1.96% of irrigation water withdrawal (9 billion m³/year), 25.59% of livestock water use (0.7 billion m³/year), and 21.73% of municipal water use (0.8 billion m³/year)²⁶. This underscores the substantial impact of WH on Lake Tana's hydrology.

Study 3: Spatiotemporal variability of lake surface water temperature and water quality parameters and its interrelationship with water hyacinth biomass in Lake Tana, Ethiopia

Lake surface water temperature (LSWT) varies significantly across regions and seasons, with higher values along the shorelines and in the southern, southwestern, and eastern areas, and lower values in the central and northern regions (Figure 3).

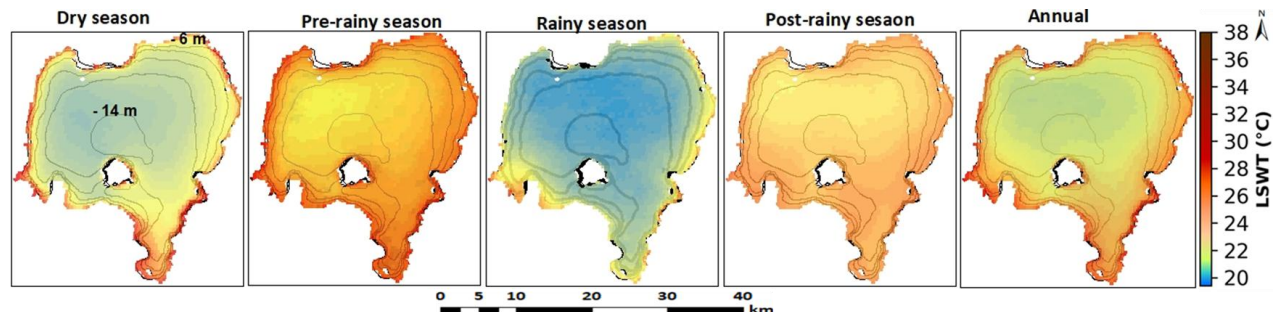


Figure 3. Mean seasonal and annual spatial distribution of lake surface water temperature (LSWT) from MODIS Terra (2001–2022) along depth contour at two-meter (2 m) intervals across the dry (December–February), pre-rainy (March–May), rainy (June–August), and post-rainy (September–November) seasons

Dense WH mats raise water temperature by reducing water movement and increasing lake water residence time. The spatial average LSWT of the lake exhibited significant decreasing trends at rates of 0.012 °C/year, 0.016 °C/year, 0.013 °C/year, and 0.012 °C/year in the pre-rainy, rainy, and post-rainy seasons, and annually, respectively. Overall, LSWT trends decreased, which could be attributed to reductions in regional air temperatures, land surface temperatures, and the Pacific Ocean Niño 3.4 SSTa.

The spatial distribution of turbidity and Chl-*a* index showed that the northern, eastern, and southwestern areas had the highest values, while central regions had the lowest. Turbidity and Chl-*a* index peaked during the rainy season and were lowest in the dry season. Predicted turbidity levels for June 2023 ranged from 4.35 to 81.60 NTU, and Chl-*a* concentrations from 6.50 to 150.20 µg/L, with high levels in the northeastern and southwestern regions (Figure 4). The turbidity index decreased significantly during the dry, rainy, and post-rainy seasons, while the pre-rainy season exhibited a non-significant decreasing trend. The Chl-*a* index decreased significantly during the pre-rainy and rainy seasons but showed non-significant increases in the dry and post-rainy seasons. Overall, the spatial average turbidity and Chl-*a* index decreased from January 2016 to February 2023, which could be linked to the expansion of WH and other aquatic vegetation that efficiently absorb nutrients and filter suspended solids⁹.

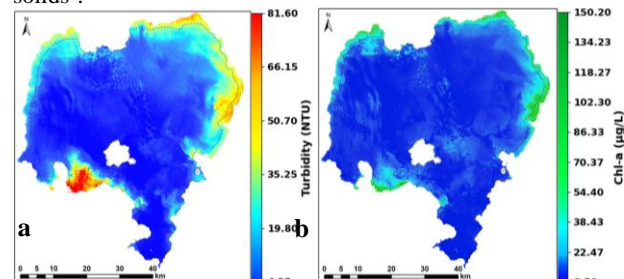


Figure 4. Predicted (a) turbidity and (b) Chl-*a* concentrations of Lake Tana (June 2023). The black dotted lines on the maps indicate depth contours at 5 meters.

The spatial average WH biomass increased in all months except May, with significant increases observed only in January and September. WH biomass had a weak, non-significant positive correlation with LSWT ($r = 0.18$). In contrast, it exhibited significant negative correlations with turbidity ($r = -0.33$) and the Chl-*a* index ($r = -0.35$), suggesting that increased WH biomass could reduce both turbidity and Chl-*a* levels ($P < 0.05$).

The highest spatial average LSWT (22.34°C) was observed in the pre-rainy season, while the lowest was during the rainy season (20.07°C). LSWT trends varied by region and season, with increasing trends in the northeastern, northwestern, and southwestern areas, and decreasing trends in the central, western, and southern regions. LSWT has consistently increased in the northeastern (WH-infested) areas across all seasons, likely due to WH's spread over the past decade.

4. Conclusion

All methods—CART, RF, and SVM—achieved >95% overall accuracy with Sentinel-2 images and > 90% with Landsat 8 images. For WH detection, all methods achieved an F1 score > 93% with both datasets. The average overall accuracy of the classifiers when using the Sentinel 2 images was 97.8%, while the average overall accuracy of the classifiers when using the Landsat 8 images was 95.5%. Although the performance differences between methods were small, RF was the most accurate compared to SVM and CART. Additionally, the post-rainy season was found to be the most effective time for WH detection in Lake Tana (Study 1). The study revealed that the spatial coverage and biomass of WH increased from 2015 to 2023, with the highest WH population observed in the northeastern sector of the lake. Concurrently, water loss due to WH evapotranspiration increased significantly, totaling approximately 176 million m³ from October 2015 to December 2023, equivalent to 0.61% of the lake's volume (Study 2). High spatiotemporal variability was observed in LSWT, turbidity, and Chl-*a*, with overall decreasing trends. WH biomass showed a weak, non-significant positive correlation with LSWT but significant negative correlations with turbidity and Chl-*a*, suggesting that WH biomass slightly increases LSWT and reduces turbidity and phytoplankton biomass in the lake (Study 3). The findings suggest integrated management strategies to balance WH's ecological and hydrological impacts and its role in water purification. The results will be vital in decision support systems and preparing strategic plans for sustainable water resource management, environmental protection, and pollution prevention.

References

- [1] Thamaga and Dube(2018) Remote Sens. Appl.Soc. Environ. 10, 36–46 [2] Tibebe et al. (2019) Microchem. J. 148, 374–384 [3] Cai et al. (2023) Limnology 24, 51–60 [4] Coetzee et al. (2014) Biodivers. Conserv. 23, 1319–1330 [5] Téllez et al. (2008) Aquat. Invasions 3, 42–53 [6] Dersseh et al (2020) Water (Switzerland) 12 [7] Damtie et al. (2022) All Life 15, 1126–1140 [8] Damtie et al. (2021) Heliyon 7, e08196 [9] Villamagna and Murphy (2010) Freshw. Biol. 55, 282–298 [10] Brendonck et al. (2003) Arch. fur Hydrobiol. 158, 389–405 [11] Aguilar-Lome et al. (2021) J. South Am. Earth Sci. 112 [12] Kayalik and Çorumluoğlu (2022) Int. J. Environ. Geoinformatics 9, 35–45 [13] Patra et al. (2017) Spat. Inf. Res. 25, 75–87 [14] Gholizadeh et al. (2016) Sensors (Switzerland) 16 [15] Xie et al. (2022) Sci. Rep. 12, 1–13 [16] Kislik et al. (2022) Ecol. Indic. 140, 109041 [17] Pham et al. (2020) Remote Sens. 12, 1–24 [18] Sun et al. (2019) Remote Sens. 11, 1–22 [19] Abebe et al. (2023) Appl. Water Sci. 13, 1–16 [20] Barclay Shoemaker and Sumner (2006) Wetlands 26, 528–543 [21] Doorenbos and Pruitt (1977) FAO Irrigation and Drainage Paper 24, 144 [22] Teshome and Amente (2022) J. Equity Sci. Sustain. Dev. 5(2), 62–82 [23] Rashed (2014) Egypt. J. Aquat. Res. 40, 117–124 [24] Muehaye et al. (2022) Remote Sens. 14 [25] Nurhusein (2020) J. Water Resour. Prot. 12, 183–202 [26] FAO (2016) Rome, Italy